

Intergranular Corrosion of Cu-Al-Ni Alloy in 0.5 mol dm⁻³ H₂SO₄ Solution

L. Vrsalović,^{a*} S. Gudić,^a L. Terzić,^a I. Ivanić,^b
S. Kožuh,^b M. Gojić,^b and E. E. Oguzie^c

^aUniversity of Split, Faculty of Chemistry and Technology, Department of Electrochemistry and Materials Protection, Ruđera Boškovića 35, 21 000 Split, Croatia

^bUniversity of Zagreb, Faculty of Metallurgy, Department of Physical Metallurgy, Aleja narodnih heroja 3, 44 000 Sisak, Croatia

^cFederal University of Technology Owerri, Africa Centre of Excellence in Future Energies and Electrochemical Systems (ACE-FUELS), PMB 1526, Owerri, Nigeria

This work is licensed under a Creative Commons Attribution 4.0 International License



Abstract

The corrosion behaviour of Cu-Al-Ni alloy in 0.5 mol dm⁻³ H₂SO₄ solution was investigated by electrochemical methods including open circuit potential measurement, electrochemical impedance spectroscopy measurements, linear and potentiodynamic polarization. Measurements were performed in 0.5 mol dm⁻³ H₂SO₄ at temperatures 20 and 40 °C. After polarization testing, corroded electrode surfaces were ultrasonically cleaned in deionized water and examined by light and scanning electron microscopy, while the elemental composition at individual points of the alloy surface was determined by EDS analysis. The results of the investigations revealed the occurrence of intergranular corrosion on the Cu-Al-Ni surface, which became more pronounced with increasing temperature.

Keywords

Shape memory alloy, Cu-Al-Ni alloy, corrosion, polarization, SEM/EDS

1 Introduction

Cu-Al-Ni alloys belong to the group of shape memory alloys (SMAs), a relatively new class of functional materials that can change from one crystallographic structure to another, in response to temperature changes or to other applied stresses.¹⁻⁴ If such alloys are plastically deformed at low temperature, they will completely recover their original shape when raised to a higher temperature. In the process of recovering their shape, these alloys can produce a displacement or a force as a function of temperature. This unique effect of returning to an original geometry after a large inelastic deformation is known as the shape memory effect (SME). The shape memory phenomenon results from crystalline phase changes known as “thermoelastic martensitic transformation”. At temperatures below the transformation temperature, shape memory alloys are martensitic. In this condition, their microstructure is characterized by “self-accommodating twins”. The martensite is soft and can easily be deformed by de-twinning. Heating above the transformation temperature converts the material to its high strength, austenitic phase.⁵⁻⁸

Ni-Ti alloys are one of the most commonly used shape memory alloys in practice due to their outstanding properties, such as excellent shape memory effect, unique superelasticity, low elastic modulus, high corrosion resistance and biocompatibility.⁹⁻¹¹ Their disadvantages lie in their high production costs and low transformation temperature

range (–100 to 100 °C), which is why they are now being replaced by cheaper alternatives like Cu-SMA alloys, for less demanding applications. The main advantages of Cu-Al-Ni alloys are their low price, relatively simple fabrication procedure, better machinability, better work/cost ratio, and high electrical and thermal conductivity compared to other shape memory alloys.^{4,5,12-15} Also, the stability of the two-way shape memory effect, which is very important in its application as actuators, is superior to that of Ni-Ti alloy.¹⁶ Actuators based on Cu-Al-Ni alloy have been tested for usage as prosthetic actuators, and also actuators made from Cu-Al-Ni single crystals (produced by Nimesis Special Industries) have been reported by NASA to be very good candidates for space applications that need trigger temperatures between 100 and 200 °C.¹⁷⁻¹⁸ Besides usage in the production of actuators, Cu-Al-Ni shape memory alloys have found their applications in various engineering devices, sensors, automotive and aerospace industries, robotics, etc.^{3,12,13,19}

Most studies on Cu-Al-Ni shape memory alloys have focused on their microstructure, mechanical and shape memory properties, and possible fields of application, but have neglected their corrosion behaviour, which is very vital for their practical use. The corrosion resistance of Cu-Al alloys has been attributed to the formation of a protective layer of alumina along with copper chlorides and oxides on the alloy surface.^{20,21} Aluminium has a greater affinity towards oxygen than copper, and higher stability of the Al₂O₃ than Cu₂O. Some researchers have attributed the enhanced corrosion resistance to the formation of duplex-layered surface oxides composed of Cu₂O × Al₂O₃ × xH₂O.²² The

* Corresponding author: prof. dr. sc. Ladislav Vrsalović
Email: ladislav@ktf-split.hr

presence of nickel is also important in the passivation of CuNi alloys because of its incorporation in the Cu(I) oxide, which reduces the number of cation vacancies that normally exist in Cu(I) oxides.^{20,21,23}

Again, a large number of the publications related to the corrosion properties of Cu-Al-Ni alloys have focused on the influence of chloride ions on the corrosion behaviour of Cu-Al-Ni alloys.^{4,6,7,23-25} The present investigation aims to determine the corrosion behaviour of Cu-Al-Ni alloy in 0.5 mol dm⁻³ H₂SO₄ solution.

2 Experimental

2.1 Materials and test solution

The investigated Cu-Al-Ni alloy, composed of 83.1 % Cu, 12.8 % Al, and 4.1 % Ni in wt%, was produced by melting pure components (Cu, Al, and Ni) in a vacuum induction furnace in a protective argon atmosphere. The melting furnace was connected to a device for continuous vertical casting, so the melting and casting of the alloy was carried out in an argon protective atmosphere. The resulting 8 mm diameter bars were cut with a precision Isomet cutter made by Buehler USA to small rollers, 1 cm in height. The preparation of the electrodes for electrochemical measurements consisted of soldering Cu-Al-Ni alloy rollers to insulated copper wires, followed by their insulation with Polyrepar S acrylate, to leave only one non-insulated roller base of 0.502 cm² bare, to be used as working electrode surface in contact with the electrolyte.

Mechanical preparation of samples before each experiment involved wet grinding of electrode surfaces with successive grades of emery papers (down to 2000 grit), using a Metkon Forcipol 1 V grinding/polishing machine. The surfaces were subsequently polished with Al₂O₃ suspension (particle size of 0.3 μm), and then ultrasonically washed in ethanol solution and with deionized water.

The 0.5 mol dm⁻³ H₂SO₄ was prepared from the 96 % H₂SO₄ obtained by Kemika.

2.2 Electrochemical measurements

The electrochemical experiments were carried out in a three-electrode glass cell in which Cu-Al-Ni electrode served as a working electrode, saturated calomel electrode as reference electrode and platinum sheet electrode as an auxiliary electrode. The electrochemical cell was a jacketed model available for temperature control by connecting to a Huber Kiss circulator. A PAR 273A potentiostat/galvanostat connected to a PAR M5210 lock-in amplifier was used for all electrochemical measurements. The open circuit potential measurements (E_{OC}) were recorded in 60 min time period immediately after electrode immersion in the electrolyte. Electrochemical impedance spectroscopy measurements were performed at E_{OC} in a frequency interval from 0.01 Hz to 50 kHz using the signal amplitude of 10 mV. Linear polarization measurements were performed with the scanning rate of 0.2 mV s⁻¹ in the potential region

of ±20 mV around the corrosion potential, while potentiodynamic polarization experiment was performed in a wide potential range (-0.250 V (vs. E_{OC}) to 1.250 V), at a scan rate of 0.5 mV s⁻¹.

2.3 Surface study

Corrosion surface morphology, after potentiodynamic polarization measurements, was investigated using an optical microscope MXFMS-BD (Ningbo Sunny Instruments Co.) and with the scanning electron microscope TESCAN VEGA TS 5136 MM equipped with an EDS system for elemental analysis.

3 Results and discussion

The open circuit potential of Cu-Al-Ni alloy in 0.5 mol dm⁻³ H₂SO₄ solution was measured immediately after immersion of the electrode in the solution at temperatures of 20 °C and 40 °C. The obtained E_{OC} vs. time plots are shown in Fig. 1.

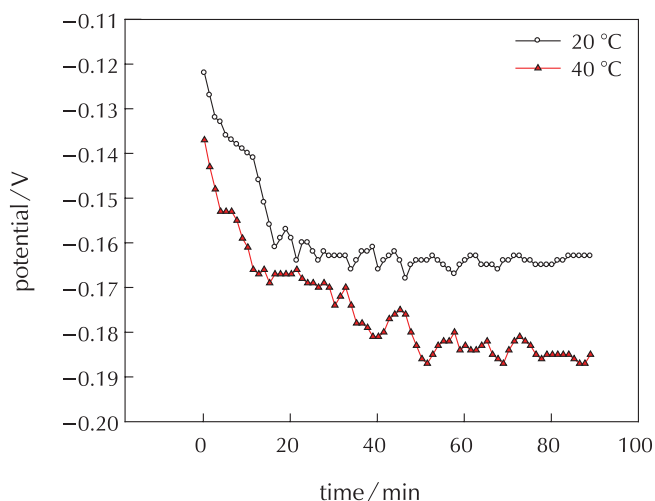


Fig. 1 – Open circuit potential measurements for Cu-Al-Ni alloy in 0.5 mol dm⁻³ H₂SO₄ solution at 20 °C and 40 °C

Slika 1 – Mjerenje potencijala otvorenog strujnog kruga za leguru Cu-Al-Ni u 0.5 mol dm⁻³ otopini H₂SO₄ pri 20 °C i 40 °C

Fig. 1 shows that, upon immersion of the electrode in the electrolyte solution, the open circuit potential changed towards negative values with some occasional instability, which can be explained by the dissolution of the air-formed Cu and Al oxides on the surface of the alloy.²⁶ The open circuit potential values for Cu-Al-Ni alloy are more negative when measured at 40 °C, indicating a negative influence of temperature on the corrosion susceptibility of the alloy. After a certain time, changes in the open circuit potential had reduced, and a stable value was established.

Electrochemical impedance spectra were taken immediately after the open circuit potential measurements of

the Cu-Al-Ni electrode in H₂SO₄ solution at 20 and 40 °C. The obtained results are presented in Fig. 2 in Nyquist and Bode plots. The lines in Fig. 2 represent the modelled data, and symbols represent experimental data.

The Nyquist diagram (Z_{imag} vs. Z_{real}) of the Cu-Al-Ni electrode in H₂SO₄ at both temperatures show fragments of a large incomplete semicircle, which are of typical impedance response for corrosion surface film, which mostly consists of cuprous and aluminium oxides.^{22,27}

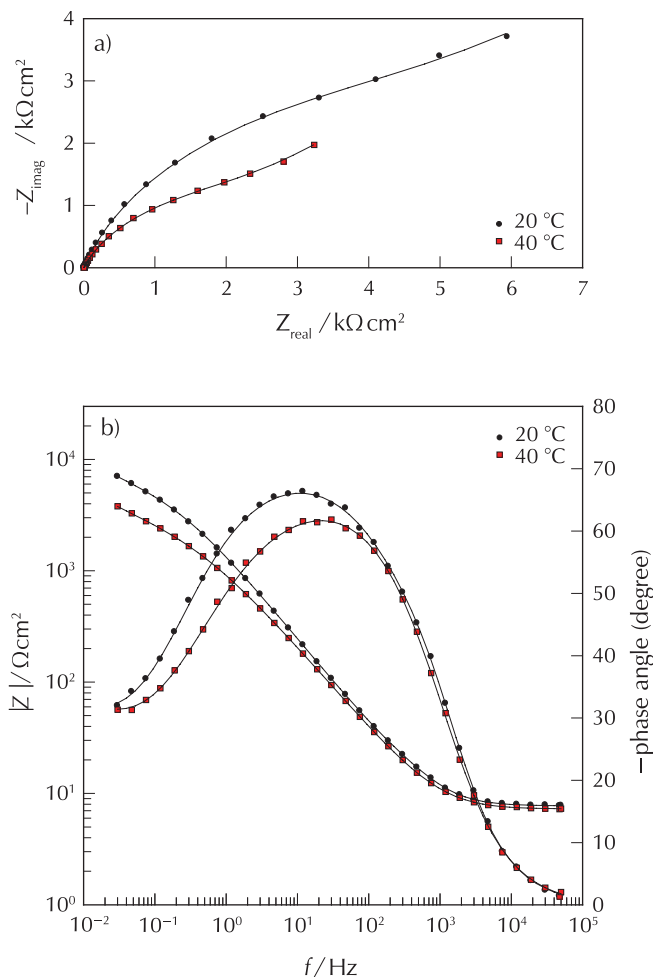


Fig. 2 – Nyquist plot (a) and Bode plot (b) for Cu-Al-Ni alloy in 0.5 mol dm⁻³ H₂SO₄ solution at 20 °C and 40 °C

Slika 2 – Niquistov (a) i Bodeov (b) prikaz za leguru Cu-Al-Ni u 0,5 mol dm⁻³ otopini H₂SO₄ pri 20 °C i 40 °C

In the Bode format (logarithm of impedance, Z , and phase angle respectively vs. logarithm of frequency, f) at high frequencies ($f > 1$ kHz), the impedance response is dominated by the electrolyte resistance. In the medium frequency region, the linear log $|Z|$ vs. log f relationship with a slope close to -1 and a phase angle of $\approx -70^\circ$, reflect the capacitive behaviour of the system. At low frequency, the

slope of ≈ -0.5 and the phase angle of $\approx -30^\circ$ point towards the presence of a slow diffusion process. The overall impedance of the system and hence corrosion resistance of the alloy, decreases with increasing temperature, indicating that the electrode surface gets less protection.

The impedance response also shows more than one time constant, which reflects the diversity of the interfacial phenomena in the system under investigation. Fig. 3 shows the equivalent circuit proposed to fit the experimental data, which consists of an electrolyte resistance R_{el} ($\approx 7 \Omega \text{cm}^2$) connected with two time constants. The first time constant observed in the high frequency region results from the fast charge transfer process in the metal dissolution reaction. In this case, R_1 represents the charge transfer resistance, and Q_1 represents the constant phase element and replaces the capacitance of the electrical double layer. To account for the surface layer of corrosion products and diffusion process in the low frequency region, additional equivalent circuit parameters were introduced, such as R_2 for the surface layer resistance, Q_2 for constant phase element of the surface layer (Q_2 replaces the capacitance of surface layer), and a Warburg impedance W for the diffusion process.

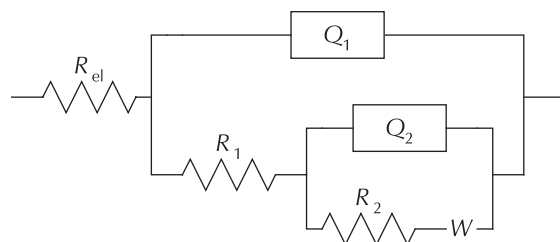


Fig. 3 – Proposed equivalent circuits for modelling the impedance data

Slika 3 – Predloženi ekvivalentni krug za modeliranje impedancijskih podataka

The constant phase element is related to the impedance, Z_{CPE} , according to Eq. (1):²⁷

$$Z_{\text{CPE}} = [Q(j\omega)^n]^{-1} \quad (1)$$

where the constant Q accounts for a combination of properties related to both the surface and the electroactive species; $j\omega$ is the complex variable for sinusoidal perturbation with $\omega = 2\pi f$, and n is the exponent of CPE.

CPEs are used in the analysis of impedance data to account deviations that occurred by surface roughness on a microscopic level. For a smooth electrode, n approaches the unity and CPE is equivalent to a capacitor. Porous surfaces show lower n values.

The parameters of the equivalent circuit were evaluated using a simple least square fit procedure, and are presented in Table 1.

Table 1 – Impedance parameters of Cu-Al-Ni alloy in 0.5 M H₂SO₄ solutionTablica 1 – Impedancijski parametri za Cu-Al-Ni leguru u 0,5 M otopini H₂SO₄

T/°C	R _{el} /Ω cm ²	Q ₁ · 10 ⁶ / Ω ⁻¹ s ⁿ cm ⁻²	n ₁	R ₁ /Ω cm ²
20	7.73	48.36	0.90	34.61
40	7.24	62.54	0.88	18.05
T/°C	Q ₂ · 10 ⁶ / Ω ⁻¹ s ⁿ cm ⁻²	n ₂	R ₂ /kΩ cm ²	W · 10 ⁴ / Ω ⁻¹ s ⁿ cm ⁻²
20	122.61	0.70	6.07	5.73
40	205.59	0.62	3.14	9.46

The results obtained indicate that an increase in electrolyte temperature leads to a corresponding decrease in charge transfer resistance (R₁) and surface layer resistance (R₂), while the capacitance of the double layer (Q₁), the capacitance of the surface layer (Q₂) and the diffusion element (W) increase. This direction of change is attributed to the negative influence of temperature increase on the protective properties of the electrode/solution interphase.

Polarization measurements were conducted in a narrow range of potentials, around E_{OC} (±20 mV), to determine the values of polarization resistance that corresponds to the corrosion resistance of the alloy. The values of the polarization resistance were determined from the slopes of the linear part of the curves shown in Table 2. Thereafter, potentiodynamic polarization measurements were performed over a wide range of potentials (from -250 mV to 1.250 V) to determine the corrosion parameters. The results are shown in Fig. 4.

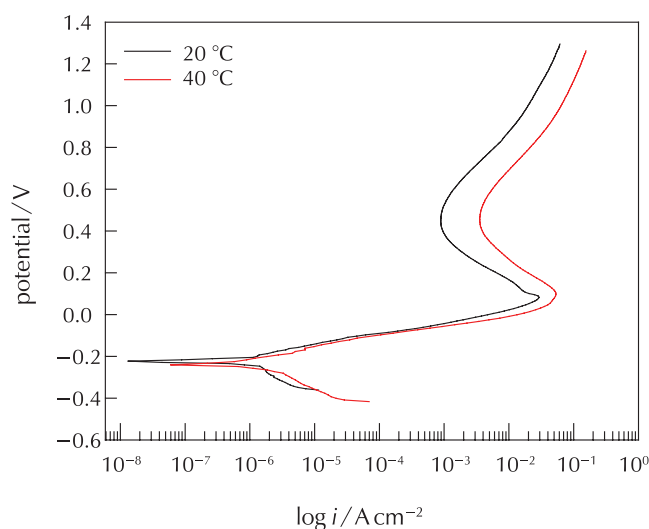
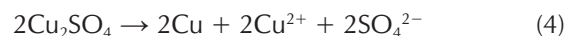
Fig. 4 – Potentiodynamic polarization curves for Cu-Al-Ni alloy in 0.5 mol dm⁻³ H₂SO₄ solution at 20 °C and 40 °CSlika 4 – Potenciodinamičke polarizacijske krivulje za leguru Cu-Al-Ni u 0,5 mol dm⁻³ otopini H₂SO₄ pri 20 °C i 40 °C

Fig. 4 reveals that the anodic parts of the curve have a so-called “S-shaped” profile²⁸, and can be divided into three separate areas; the Tafel region, the pseudo-passive area where the maximum and minimum anode current density occur (i.e., the decrease in the value of the anode current density due to the formation of a surface layer of corrosion products that slow down the alloy dissolution process), and a third region where the anode current density increases again.²⁶ Similar polarization behaviour was observed for Cu-Al-Ni alloy in NaCl solutions.^{4,6,24} The slope of the anode Tafel direction of about 60 mV dec⁻¹ suggests that the anodic process is determined by the diffusion of soluble compounds from the electrode surface into the bulk of the solution.²⁰ Awad and associates²⁹ have proposed the following copper dissolution mechanism:



The adsorption of sulphate on the copper surface over a wide range of anode potentials has been experimentally demonstrated.³⁰ According to this mechanism, which has been accepted by some other authors, the disproportionation of adsorbed Cu (I) compounds leads to the formation of soluble Cu (II) compounds.

Corrosion parameters were determined from the polarization curves shown in Table 2.

Table 2 – Corrosion parameters from the polarization measurements

Tablica 2 – Korozijski parametri određeni polarizacijskim mjerenjima

T/°C	R _p /Ω cm ²	i _{corr} /μA cm ⁻²	E _{corr} /V	v _{corr} /mm a ⁻¹
20	6410	1.46	-0.210	0.0199
40	3462	2.92	-0.231	0.0398

Corrosion rate v_{corr} was calculated according to ASTM G 59-97 standard procedure,³¹ wherein the corrosion rate (mm per year) can be determined from Eq. (5), in which E.W. is the equivalent weight of the corroding species in grams, and ρ is the density of the corroding material in g cm⁻³.

$$v_{\text{corr}} = 3.27 \cdot 10^{-3} \cdot (i_{\text{corr}}/\rho) \cdot \text{E.W.} \quad (5)$$

From Table 2, it can be seen that increasing the electrolyte temperature leads to an increase in corrosion current density and a decrease in polarization resistance, corresponding to more severe corrosion of the Cu-Al-Ni alloy.

After potentiodynamic polarization measurements, the corroded Cu-Al-Ni electrodes were cleaned thoroughly in deionized water in an ultrasonic bath, dried, and examined using a light microscope in the dark field mode (Fig. 5). The images show intense corrosion at the grain boundaries (intergranular corrosion), which in some places goes into localized corrosion. Shallow round damage due to localized corrosion was also observed on the surface away from the grain boundaries.

After polarization measurements, a more detailed insight into the state of the electrode surfaces was obtained by SEM/EDS analysis (Figs. 6–8). Fig. 6a) and Fig. 7 show the state of the Cu-Al-Ni alloy surface after potentiodynamic polarization in 0.5 mol dm⁻³ H₂SO₄ at a temperature of 20 °C, while Fig. 6b) and Fig. 8 show the electrode surface after polarization at 40 °C.



Fig. 5 – Cu-Al-Ni alloy surface after polarization measurements in 0.5 mol dm⁻³ H₂SO₄ at 20 °C

Slika 5 – Površina legure Cu-Al-Ni nakon polarizacijskih mjerenja u 0,5 mol dm⁻³ otopini H₂SO₄ pri 20 °C

The surfaces are clearly without any corrosion products, and the images show occurrence of intense intergranular corrosion at the grain boundaries, which in some places is combined with severe localized corrosion, characterized by deep pits.

EDS analysis in marked points has shown that all alloying elements were present on the surface, with the percentage of aluminium and nickel being slightly lower than their percentage in the original alloy before corrosion dissolution. In the investigation of the corrosion behaviour of Cu-Al and Cu-Al-Be alloys in H₂SO₄ media, *Kuo et al.* had found the formation of the intergranular corrosion resulting from the preferential etching of grain boundaries when samples were polarised at 0.6 V.²⁸ Therefore, the reduction of Al content on the grain boundaries as well as on the spot nearby the grain boundary suggests preferential dissolution

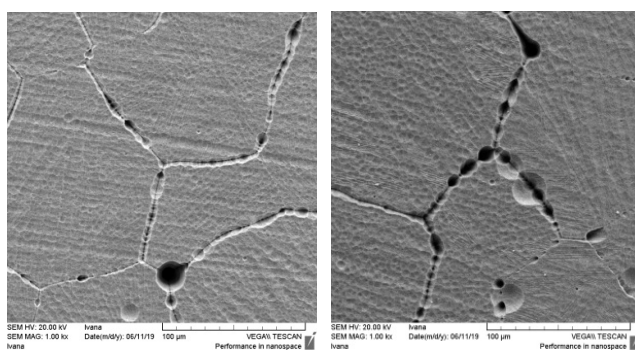


Fig. 6 – SEM images of corroded Cu-Al-Ni alloy surfaces after potentiodynamic polarization in 0.5 mol dm⁻³ H₂SO₄ solution at (a) 20 °C and (b) 40 °C

Slika 6 – SEM snimka korodirane površine Cu-Al-Ni legure nakon potenciodinamičke polarizacije u 0,5 mol dm⁻³ otopini H₂SO₄ pri 20 °C i 40 °C

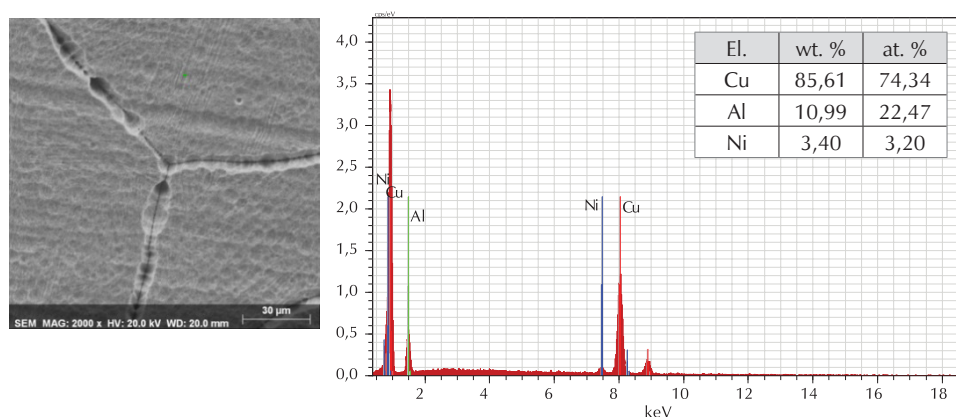


Fig. 7 – SEM/EDS analysis of corroded Cu-Al-Ni alloy surfaces after potentiodynamic polarization in 0.5 mol dm⁻³ H₂SO₄ solution at 20 °C

Slika 7 – SEM/EDS analiza korodirane površine Cu-Al-Ni legure nakon potenciodinamičke polarizacije u 0,5 mol dm⁻³ otopini H₂SO₄ pri 20 °C

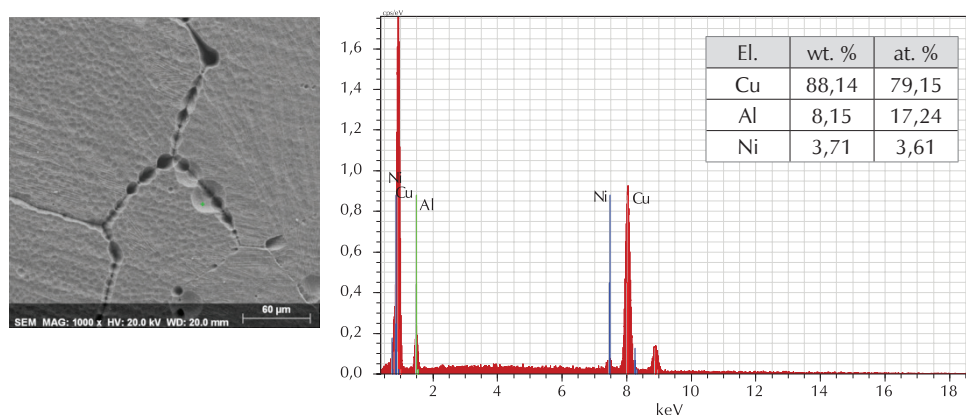


Fig. 8 – SEM/EDS analysis of corroded Cu-Al-Ni alloy surfaces after potentiodynamic polarization in 0.5 mol dm⁻³ H₂SO₄ solution at 40 °C

Slika 8 – SEM/EDS analiza korodirane površine Cu-Al-Ni legure nakon potenciodinamičke polarizacije u 0,5 mol dm⁻³ otopini H₂SO₄ pri 40 °C

of Al. It can be explain by the action of a low pH of the solution as well as high anodic potentials at which potentiodynamic polarization was performed.

4 Conclusion

Investigated was the corrosion behaviour of Cu-Al-Ni alloy in 0.5 mol dm⁻³ H₂SO₄ at (a) 20 °C and (b) 40 °C. Increasing the temperature led to a decrease in the polarization resistance value and an increase in the corrosion current density value, indicating more intense corrosion of the Cu-Al-Ni alloy.

The surface image of the Cu-Al-Ni alloy after polarization measurements by light and SEM microscopy indicated the appearance of intergranular corrosion along with pitting corrosion. Increasing the electrolyte temperature led to greater damages to the surface.

EDS elemental surface analysis at a certain point revealed the presence of all alloying elements on the surface. At higher temperatures, the copper content was slightly higher and the aluminium content lower, which could indicate its higher dissolution from the surface.

List of abbreviations and symbols

Popis kratica i simbola

SMA _s	– shape memory alloys – legure s prisjetljivosti oblika
SEM	– scanning electron microscopy – pretražna elektronska spektroskopija
EDS	– energy dispersive spectroscopy – energijski disperzivna spektroskopija
E _{OC}	– open circuit potential, V – potencijal otvorenog strujnog kruga, V

Z	– impedance, kΩ – impedancija, kΩ
f	– frequency, Hz – frekvencija, Hz
R _{el}	– electrolyte resistance, Ω cm ² – otpor elektrolita, Ω cm ²
R ₁	– charge transfer resistance, kΩ cm ² – otpor prijenosu naboja, kΩ cm ²
R ₂	– surface layer resistance, kΩ cm ² – otpor površinskog sloja, kΩ cm ²
Q	– constant phase element, Ω ⁻¹ s ⁿ cm ⁻² – konstantni fazni element, Ω ⁻¹ s ⁿ cm ⁻²
R _p	– polarization resistance, kΩ cm ² – polarizacijski otpor, kΩ cm ²
i _{corr}	– corrosion current density, μA cm ⁻² – gustoća korozijske struje, μA cm ⁻²
E _{corr}	– corrosion potential, V – korozijski potencijal, V
v _{corr}	– corrosion rate, mm a ⁻¹ – brzina korozije, mm a ⁻¹
ρ	– density of the corroding material, g cm ⁻³ – gustoća korodiranog materijala, g cm ⁻³
E.W.	– equivalent weight of the corroding species, g – ekvivalentna masa korodiranog materijala, g

References

Literatura

1. M. Čolić, R. Rudolf, D. Stamenković, I. Anžel, D. Vučević, M. Jenko, V. Lazić, G. Lojen, Relationship between microstructure, cytotoxicity and corrosion properties of Cu-Al-Ni shape memory alloy, *Acta Biomater.* **6** (1) (2010) 308–317, doi: <https://doi.org/10.1016/j.actbio.2009.06.027>.
2. I. Ivanić, M. Gojić, S. Kožuh, Slitine s prisjetljivosti oblika (I. dio): najznačajnija svojstva (Shape Memory Alloys (Part I): Significant Properties), *Kem. Ind.* **63** (9-10) (2014) 323–330, doi: <https://doi.org/10.15255/KUI.2013.016>.

3. R. Dasgupta, A look into Cu-based shape memory alloys: Present scenario and future prospects, *J. Mater. Res.* **29** (16) (2014) 1681–1698, doi: <https://doi.org/10.1557/jmr.2014.189>.
4. L. Vrsalović, I. Ivanić, S. Kožuh, S. Gudić, B. Kosec, M. Gojić, Effect of heat treatment on corrosion properties of CuAlNi shape memory alloy, *Trans. Nonferrous Met. Soc. China.* **28** (6) (2018) 1149–1156, doi: [https://doi.org/10.1016/S1003-6326\(18\)64752-1](https://doi.org/10.1016/S1003-6326(18)64752-1).
5. A. C. Kneissl, E. Unterweger, M. Bruncko, G. Lojen, K. Mehraibi, H. Scherngell, Microstructure and properties of NiTi and CuAlNi shape memory alloys, *MJoM* **14** (2) (2008) 89–100.
6. M. Gojić, L. Vrsalović, S. Kožuh, A. Kneissl, I. Anžel, S. Gudić, B. Kosec, M. Kliškić, Electrochemical and microstructural study of Cu-Al-Ni shape memory alloy, *J. Alloy. Compd.* **509** (41) (2011) 9782–9790, doi: <https://doi.org/10.1016/j.jallcom.2011.07.107>.
7. S. N. Saud, E. Hamzah, T. Abubakar, H. R. Bakhsheshi-Rad, Correlation of microstructural and corrosion characteristics of quaternary shape memory alloys Cu-Al-Ni-X (X=Mn or Ti), *Trans. Nonferrous Met. Soc. China* **25** (4) (2015) 1158–1170, doi: [https://doi.org/10.1016/S1003-6326\(15\)63711-6](https://doi.org/10.1016/S1003-6326(15)63711-6).
8. X. Hou, Design, fabrication, properties and application of smart and advanced materials, CRC Press, New York, USA, 2016.
9. T. Kanemura, K. Yokoyama, J. Sakai, Effect of acid type on corrosion and fracture behavior of Ni-Ti superelastic alloy under sustained tensile load in a physiological saline solution containing hydrogen peroxide, *Corros. Sci.* **50** (10) (2008) 2785–2795, doi: <https://doi.org/10.1016/j.corsci.2008.07.018>.
10. S. Kožuh, L. Vrsalović, M. Gojić, S. Gudić, B. Kosec, Comparison of the corrosion behavior and surface morphology of NiTi alloy and stainless steels in sodium chloride solution, *J. Min. Metall. B* **52** (1) (2016) 53–61, doi: <https://doi.org/10.2298/JMMB150129003K>.
11. M. Mehrpouya, H. C. Bidsorkhi, MEMS Applications of NiTi based shape memory alloys: a review, *Micro and Nanosystems*, **8** (2) (2016) 79–91, doi: <https://doi.org/10.2174/1876402908666161102151453>.
12. I. Ivanić, M. Gojić, S. Kožuh, Slitine s prisjetljivosti oblika (II. dio): podjela, proizvodnja i primjena (Shape memory alloys (Part II): Classification, Production and Application), *Kem. Ind.* **63** (9-10) (2014) 331–344, doi: <https://doi.org/10.15255/KUI.2013.017>.
13. S. N. Saud Al-Humairi, Cu-based shape memory alloys: modified structures and their related properties, 2019., doi: <https://doi.org/10.5772/intechopen.86193>.
14. G. Lojen, M. Gojić, I. Anžel, Continuously cast Cu-Al-Ni shape memory alloy – Properties in as-cast condition, *J. Alloy. Compd.* **580** (2013) 497–504, doi: <https://doi.org/10.1016/j.jallcom.2013.06.136>.
15. I. Ivanić, S. Kožuh, T. Holjevac Grgurić, B. Kosec, M. Gojić, The influence of heat treatment on microstructure and phase transformation temperatures of Cu-Al-Ni shape memory alloy, *Kem. Ind.* **68** (3-4) (2019) 111–118, doi: <https://doi.org/10.15255/KUI.2018.037>.
16. H. Scherngell, A. C. Kneissl, Generation, development and degradation of the intrinsic two-way shape memory effect in different alloy systems”, *Acta Mater.* **50** (2) (2002) 327–341, doi: [https://doi.org/10.1016/S1359-6454\(01\)00342-1](https://doi.org/10.1016/S1359-6454(01)00342-1).
17. C. M. Lucas dos Santos, F. Leite da Cunha, V. I. Dynnikov, The application of shape memory actuators in anthropomorphic upper limb prostheses, *Artifi. Org.* **27** (5) (2003) 473–477, doi: <https://doi.org/10.1046/j.1525-1594.2003.07242.x>.
18. A. Hautcoeur, F. Fouche, J. Sicre, Cu-Al-Ni shape memory single crystal wires with high transformation temperatures, In: 43rd Aerospace Mechanisms Symposium, NASA Ames Research Center, Moffett Field, CA, United States, May 4–6, 2016, doi: <https://ntrs.nasa.gov/search.jsp?R=20160008130>.
19. M. Sreekumar, T. Nagarajan, M. Singaperumal, Critical review of current trends in shape memory alloy actuators for intelligent robots, *Ind. Robot: Int. J.* **34** (4) (2007), 285–294, doi: <https://doi.org/10.1108/01439910710749609>.
20. A. V. Benedetti, P. T. A. Sumodjo, K. Nobe, P. L. Cabot, W. G. Proud, Electrochemical studies of copper, copper-aluminium and copper-aluminium-silver alloys: impedance results in 0.5 M NaCl, *Electrochim. Acta* **40** (16) (1995) 2657–2668, doi: [https://doi.org/10.1016/0013-4686\(95\)00108-Q](https://doi.org/10.1016/0013-4686(95)00108-Q).
21. W. A. Badawy, R. M. El-Sherif, H. Shehata, Electrochemical stability of Cu-10Al-5Ni alloy in chloride-sulphate electrolytes, *Electrochim. Acta* **54** (19) (2009) 4501–4505, doi: <https://doi.org/10.1016/j.electacta.2009.03.040>.
22. W. A. Badawy, M. M. El-Rabiee, N. H. Helal, H. Nady, Synergistic effects of alloying elements in Cu-ternary alloys in chloride solutions, *Electrochim. Acta*, **120** (1) (2014) 39–45, doi: <https://doi.org/10.1016/j.electacta.2013.12.043>.
23. H. Nady, N. H. Helal, M. M. El-Rabiee, W. A. Badawy, The role of Ni content on the stability of Cu-Al-Ni ternary alloy in neutral chloride solution, *Mater. Chem. Phys.* **134** (2-3) (2012) 945–950, doi: <https://doi.org/10.1016/j.matchemphys.2012.03.096>.
24. L. Vrsalović, I. Ivanić, D. Čudina, L. Lokas, S. Kožuh, M. Gojić, The influence of chloride ion concentration on the corrosion behavior of the CuAlNi alloy, *Techn. J.* **11** (3) (2017) 67–72.
25. S. N. Saud, E. Hamzah, T. Abubakar, H. R. Bakhsheshi-Rad, Microstructure and corrosion behaviour of Cu-Al-Ni shape memory alloys with Ag nanoparticles, *Mater. Corros.* **66** (6) (2014) 527–534, doi: <https://doi.org/10.1002/maco.201407658>.
26. S. S. Rosatto, P. L. Cabot, P. T. A. Sumodjo, A. V. Benedetti, Electrochemical studies of copper–aluminum–silver alloys in 0.5 M H₂SO₄, *Electrochim. Acta* **46** (7) (2001) 1043–1051, doi: [https://doi.org/10.1016/S0013-4686\(00\)00685-X](https://doi.org/10.1016/S0013-4686(00)00685-X).
27. D. D. Raistrick, J. R. Macdonald, D. R. Franceschetti, in: Macdonald J. R. (Ed.), *Impedance Spectroscopy*, J. Wiley & Sons, New York, 1987.
28. H. H. Kuo, W. H. Wang, Y. F. Hsu, C. A. Huang, The corrosion behavior of Cu-Al and Cu-Al-Be shape memory alloys in 0.5 M H₂SO₄ solution, *Corros. Sci.* **48** (12) (2006) 4352–4364, doi: <https://doi.org/10.1016/j.corsci.2006.04.006>.
29. S. A. Awad, Kh. M. Kamel, A. El-Hadi, H. A. Bayumi, Mechanism of anodic dissolution of copper in aqueous acidified solutions of different anions, *J. Electroanal. Chem.* **199** (12) (1986) 341–350, doi: [https://doi.org/10.1016/0022-0728\(86\)80008-0](https://doi.org/10.1016/0022-0728(86)80008-0).
30. L. M. Rice-Jackson, G. Horanyi, A. Wieckowski, Radio-tracer study of adsorption of HSO₄⁻ and SO₄²⁻ ions on a smooth copper electrode in acid and neutral media, *Electrochim. Acta* **36** (5-6) (1991) 753–757, doi: [https://doi.org/10.1016/0013-4686\(91\)85270-H](https://doi.org/10.1016/0013-4686(91)85270-H).
31. ASTM G 59-97 “Standard test methods for conducting potentiodynamic polarization resistance measurements”, ASTM, 100 Barr Harbor Drive, West Conshohocken, PA 19428-2959, United States, 1997.

SAŽETAK

Interkristalna korozija Cu-Al-Ni legure u 0.5 mol dm⁻³ H₂SO₄ otopini

Ladislav Vrsalović,^{a*} Senka Gudić,^a Lana Terzić,^a Ivana Ivanić,^b
Stjepan Kožuh,^b Mirko Gojić^b i Emeka Emmanuel Oguzie^c

Korozijsko ponašanje Cu-Al-Ni legure u 0,5 mol dm⁻³ H₂SO₄ otopini ispitivano je elektrokemijskim metodama kao što su mjerenje potencijala otvorenog strujnog kruga, mjerenje metodom elektrokemijske impedancijske spektroskopije, linearne i potenciodinamičke polarizacije. Mjerenja su provedena u 0,5 mol dm⁻³ H₂SO₄ pri temperaturama od 20 i 40 °C. Nakon polarizacijskih mjerenja korodirane površine elektroda ultrazvučno su očišćene u deioniziranoj vodi i ispitane svjetlosnim i pretražnim elektronskim mikroskopom, dok je elementarni sastav na pojedinim točkama na površini određen EDS analizom. Rezultati ispitivanja pokazali su da dolazi do interkristalne korozije na površini Cu-Al-Ni legure, čiji intenzitet raste s povećanjem temperature elektrolita.

Ključne riječi

Legura s prisjetljivosti oblika, Cu-Al-Ni legura, korozija, polarizacija, SEM/EDS

^a Sveučilište u Splitu, Kemijsko tehnološki
Fakultet, Zavod za elektrokemiju i zaštitu
materijala, Ruđera Boškovića 35, 21 000 Split,
Hrvatska

^b Sveučilište u Zagrebu, Metalurški fakultet
Zagreb, Zavod za fizičku metalurgiju, Aleja
narodnih heroja 3, 44 000 Sisak, Croatia

^c Federal University of Technology Owerri, Africa
Centre of Excellence in Future Energies and
Electrochemical Systems (ACE-FUELS),
PMB 1526, Owerri, Nigerija

Izvorni znanstveni rad
Prispjelo 14. travnja 2020.
Prihvaćeno 12. svibnja 2020.